[13] DFT computations indicate that the "ligand band" lies below the "metal band" in silver fluorides;[2] for example for AgF the energy difference is some 3 eV, similar to the experimental value of 2.5 eV.
[14] J. J. Yeh, I. Lindau, *Atomic Data and Nuclear Data Tables* **1985**, *32*, 1.
[15] The ionization cross-section of the F(2s) electrons is one order of magnitude smaller than that for the Ag(4d) ones, and the contribution from the former to the valence band is small, according to the calculations[2].
[16] U. Gelius, in *Electron Spectroscopy* (Ed. D. Shirley) North Holland, Amsterdam, **1972**.
[17] This band is centered at 3.68 eV, and has a small half width of 0.74 eV and integrated intensity of 7% of the whole valence band. It has been erroneously assigned either to valence orbitals baring some O(2p) character.[4] The same peak shows at 3.78 eV (half width of 0.70 eV, integrated intensity of 7% of the whole valence band) in the spectrum of comm-AgF_2, and it certainly belongs to AgF (comm-AgF_2 is partially reduced on the surface).
[18] The "ligand band" progressively shifts to lower binding energies in the order $AgF > AgCl > AgBr \approx AgI$, and simultaneously gains intensity, thus reflecting the increasing energy of the *n*p orbitals of the nonmetal and their stronger mixing with the Ag(4d) orbitals.
[19] A. Goldmann, J. Tejeda, N. J. Shevchik, M. Cardona, *Phys. Rev. B* **1974**, *10*, 4388.
[20] J. Tejeda, N. J. Shevchik, W. Braun, A. Goldmann, M. Cardona, *Phys. Rev. B* **1975**, *12*, 1557.
[21] R. Matzdorf, A. Goldmann, *J. Electron Spectrosc. Relat. Phenom.* **1993**, *63*, 167.
[22] Note, also that the dispersion of the "ligand band" usually increases with the increase of the silver oxidation state (0.79 eV for Ag(I), 1.56 eV for $KAgF_3$, and 1.71 – 1.73 eV for AgF_2 and $KAgF_4$), due to the decreasing (shortest) F – F distance in these compounds (3.493 Å, 3.026 Å, 2.843 Å, and 2.639 Å, respectively).
[23] The values listed in Table 6 of ref.[4] were normalized so that the sum of contributions is 100%. Contributions from all silver valence orbitals (4d + 5s + 5p) was in fact taken in ref.[2]. However the contribution from Ag(5s + 5p) states to the valence band is computed to be small and can be neglected in the comparison that follows.
[24] In fact, the computation was for $CsAgF_3$ and not for $KAgF_3$, but it should not have significant impact on the quantitative comparison.
[25] The corresponding value for the comm-AgF_2 is 70:30, in between the values for AgF and for the freshly prepared AgF_2; it suggests that comm-AgF_2 is partially reduced, at least on the surface.
[26] Thus it proves not to be only a (computational) artifact of the choice of the Weigner – Seitz radii.
[27] More detailed considerations should involve the difference of the lattice energies of substrate and products.
[28] $KAgF_3$ studied here, proves to be metallic: W. Grochala, P. P. Edwards, unpublished results.
[29] http://www.dl.ac.uk/RUSTI/xps/esca300.htm
[30] *Practical Surface Analysis* (Ed. D. Briggs, M. P. Seah), Wiley, Chichester **1990**.
[31] B. Žemva, R. Hagiwara, W. J. Casteel, Jr., K. Lutar, A. Jesih, N. Bartlett *J. Am. Chem. Soc.* **1990**, *112*, 4846. AgF_2 was prepared by the reaction between $AgNO_3$ and elemental fluorine at 250 °C.
[32] R. H. Odenthal, R. Hoppe, *Monatsh. Chem.* **1971**, *102*, 1340. The procedure was modified by use of AgF_2 instead of AgF and F_2 as substrates.
[33] K. Lutar, S. Milićev, B. Žemva, B. G. Mueller, B. Bachmann, R. Hoppe, *Eur. J. Solid State Inorg. Chem.* **1991**, *28*, 1335. $KAgF_4$ was prepared by the reaction between AgF_2, KF and KrF_2 in anhydrous HF as a solvent.

Received: April 7, 2003 [Z 777]

Polarization-Dependent Surface-Enhanced Raman Spectroscopy of Isolated Silver Nanoaggregates

Hongxing Xu*[a] and Mikael Käll[b]

KEYWORDS:

nanoparticles · polarization · silver · surface-enhanced Raman scattering

Surface-enhanced Raman scattering (SERS)[1] is a vibrational spectroscopy technique based on surface plasmon enhanced optical interactions at noble-metal nanostructures. With a detection limit at the single-molecule level[2] and a power to provide structural information through the Raman "vibrational fingerprint", SERS has a unique potential for ultrasensitive molecular identification and analysis. A recent example is the detection of single-DNA and RNA strands labeled by SERS-active dye molecules.[3] Nanostructured substrates for SERS are expected to be anisotropic in terms of the local surface plasmon resonances,[4] which imply that the enhancement factor should extrinsically depend on the incident polarization. This effect is expected to be particularly strong for nanometric gaps between nanoparticles,[5] which have been implicated as the most likely sites for single-molecule SERS.[6, 7] However, most SERS studies have been performed at fixed polarization configuration and/or using macroscopic sampling volumes, for which a detailed comparison between local morphology, SERS activity and theory is difficult. Herein, we report on the polarization-dependent SERS from isolated aggregates of silver nanoparticles characterized by scanning electron microscopy (SEM). The results are found to be consistent with electrodynamic theory and strongly support the idea that nanogaps are a key ingredient of ultrasensitive SERS analysis.

SERS-active structures were prepared by aggregating colloidal Ag particles (35 pM) through incubation with excess hemoglobin (5 nM), followed by immobilization on polymer-coated Si substrates. The role of the protein is twofold: to induce nanogaps through aggregation[6] and to uniformly cover the nanoparticles with SERS-active species. The SERS structures so-formed were well separated and allowed for polarization-dependent Raman studies of isolated nanoparticle aggregates using a Renishaw 2000 micro-Raman setup operated in either spectroscopy or imaging mode.

Figure 1 gives examples of polarization-dependent SERS from two Ag dimers shown in the inset. As reported elsewhere,[6, 8, 9]

[a] *Dr. H. Xu*
Division of Solid State Physics
Lund University, Box 118 22100 (Sweden)
Fax: (+46) 46-222-3637
E-mail: hongxing.xu@ftf.lth.se

[b] *Prof. Dr. M. Käll*
Department of Applied Physics
Chalmers University of Technology
41296, Göteborg (Sweden)

 DOI: 10.1002/cphc.200200544

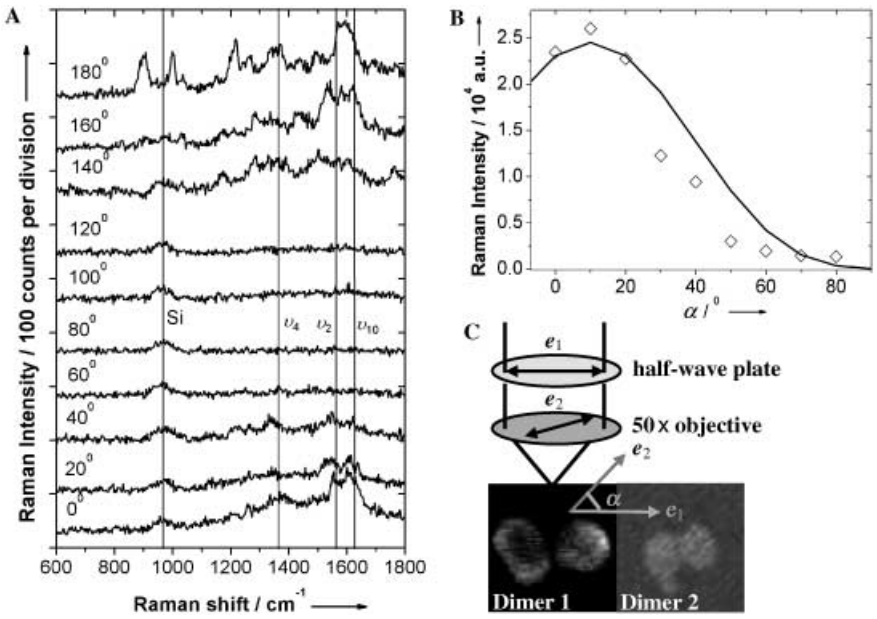

Figure 1. *Polarization-dependent SERS spectra (A) and SERS intensity (B) from the corresponding dimers shown in the SEM images (C) [Dimer 1: 285 × 285 nm² for A) and Dimer 2: 420 × 420 nm² for B)]. The half-wave plate in the inset rotates the polarization vector of the excitation beam (e_1) by an angle α but also rotates back the polarized, backscattered Raman field by the same angle, so that measurements are unaffected by the polarization-dependent response of the spectrometer. In A), vertical lines mark heme modes (ν_2, ν_4, ν_{10})[5] and the two-phonon band of the Si substrate. In B), the vertical axis shows the integrated intensity between 700 and 2200 cm⁻¹ Stokes shifts [◇ experimental data, —— fit to $\cos^4(\alpha - \alpha_0)$]. All measurements were performed using excitation at 514.5 nm and with the same collection time (30 s). The incident irradiance was ≈ 1 μW/μm² in A) and ≈ 0.1 μW/μm² in B). The angle α_0 between the dimer axis and the e_1 axis was ≈ 0° in A) and 10° in B).*

SERS spectra recorded from this type of aggregates are a superposition of heme-group modes that vary in position and intensity, possibly due to local dynamics,[10] and a fluctuating background. The latter is probably due to a photochemical degradation of the protein,[9] resulting in a spectral contribution similar to amorphous carbon.[11] Despite these spectral fluctuations, the polarization dependency of the SERS signal is clear: the Raman intensity is maximized for an incident polarization parallel to the dimer axis [($\alpha_0 \approx 0^0$ in A) and $\alpha_0 \approx 10^0$ in B)], but within the background level for the perpendicular polarization. The variation in intensity with polarization angles is well described by a $\cos^4(\alpha - \alpha_0)$ dependency, as discussed below. Both the polarized and the depolarized Raman signal (i.e., parallel and perpendicular to the incident polarization, respectively) had a similar behavior.

A rapid way to check the polarization dependency of the SERS signal is to use Raman imaging, for which many isolated SERS-structures can be investigated simultaneously. Figure 2 a shows an SEM image of Hb/Ag aggregates within one investigated area. The corresponding polarized Raman images for different angles α between the incident electric field vector and the coordinate system of the sample are shown in Figure 2 b. The Raman images revealed six bright spots above the background, marked as A to F in Figure 2 b. These could be clearly identified as different Hb/Ag aggregates in the SEM, see Figure 2 a. Structures without any detectable Raman signal turned out to be either single Ag particles or aggregates of small particles ($R < 40$ nm).

The intensities of the Raman spots in Figure 2 b obviously vary with the incident polarization. Figure 3 a shows a polar plot of this variation for spot A, a third dimer, with its axis rotated $\alpha_0 \approx 125^0$ relative to the e_1 axis. It is rather clear that the Raman intensity again has a maximum when the incident polarization is parallel to the dimer axis.

For aggregates composed of more than two particles, the polarization dependency turned out to be in general more isotropic than for isolated dimers. Figure 3 b, as an example, shows a polar plot of the Raman intensity from spot C, which was composed of five Ag particles. In this case, a large signal was observed for all polarization angles, see Figure 2 b, but with two noticeable anisotropic intensity peaks for polarization parallel to the $80^0 - 260^0$ and $160^0 - 340^0$ directions, as shown in Figure 3 b. We interpret such complicated polarization dependencies as a result of an entangled electromagnetic coupling between

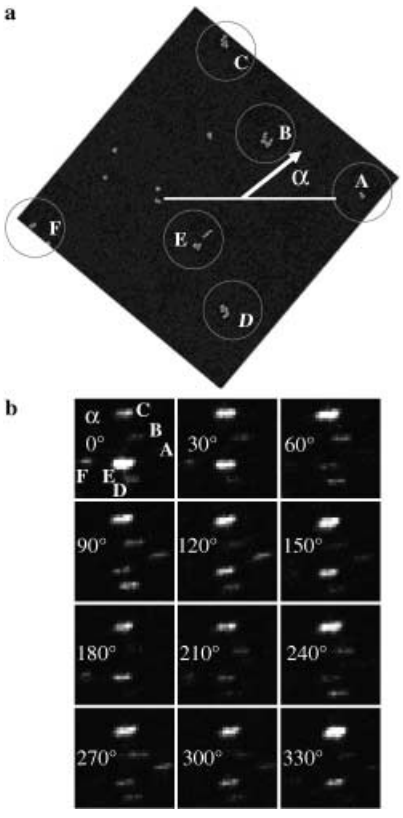

Figure 2. *a) SEM image of Hb/Ag clusters (accelerating voltage 5 kV and magnification 8500) and b) the corresponding polarized Raman images (11 × 11 μm²) for different incident polarizations α (514.5 nm, ≈ 0.1 μW/μm², intensity integrated from 700 to 2200 cm⁻¹ over 30 s per Raman image). Gold grids (100 × 100 μm² mesh) were used to mark the substrate and to identify corresponding nanoparticles in the SEM and Raman images.*

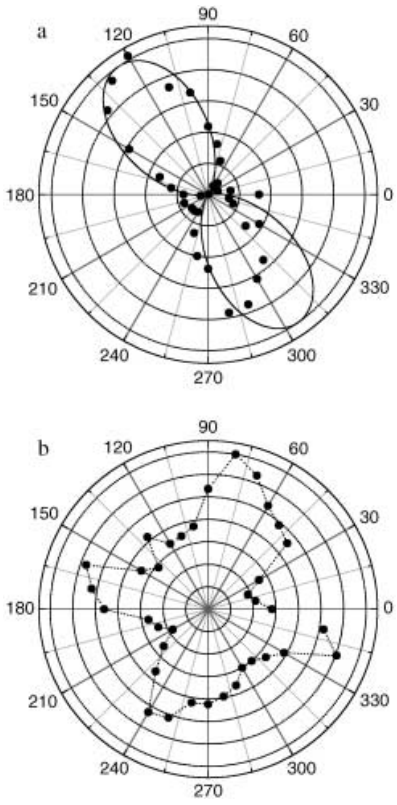

Figure 3. *Polar plots of the Raman intensity of a) spot A and b) spot C in Figure 2 versus polarization angle α (●), and fit (——) to a $\cos^4(\alpha - \alpha_o)$ dependency in a). The Raman intensity scale (a.u.) corresponds to 500 and 2000 counts per division in a) and b), respectively.*

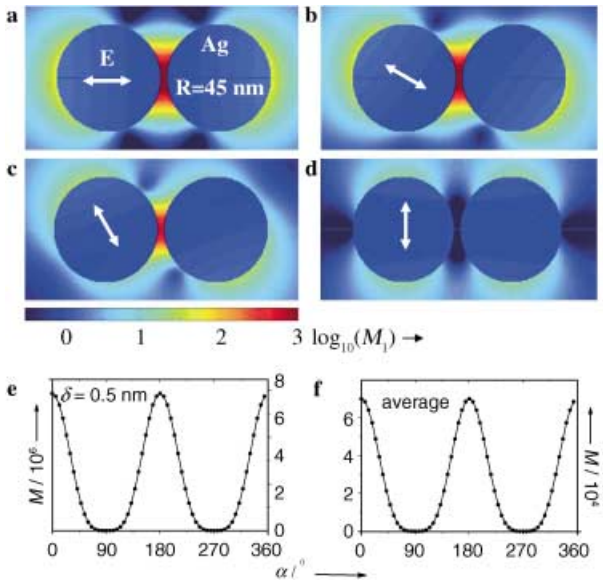

Figure 4. *Local intensity enhancement $M_1 = [E_{loc}/E_0]^2$ in logarithmic scale in a plane through the centers of the Ag spheres and perpendicular to the incident wave-vector **k** versus incident polarization: a) 0^0, b) 30^0, c) 60^0 and d) 90^0. The arrows represent the different polarizations. In e), we show the SERS enhancement factor $M = M_1^2$ (dots) as a function the incident polarization α for a point in the nanogap located at the dimer axis $\delta = 0.5$ nm away from one spherical surface, and fit (solid line) to a $\cos^4(\alpha)$ dependency. In f), we show M (●) averaged over all points $\delta = 0.5$ nm outside the Ag sphere surfaces versus α, and fit (——) to a $\cos^4(\alpha)$ dependency. The radius $R = 45$ nm corresponds to the average size of the Ag nanoparticles used in the experiment while the separation distance $d = 5.5$ nm corresponds to the diameter of a Hb molecule. The incident wavelength is 514.5 nm in all cases. Calculations were performed using a dielectric function for Ag based on experimental data.[15]*

several particles. In this particular case, the angular variation indicates an interpretation in terms of a superposed signal from two dominating but perpendicular dimers within the five-particle aggregate.

SERS originates in localized surface plasmon resonances, which enhance optical interactions at the nanoparticle surface. It is generally agreed that the main part of this effect can be rationalized in terms of an electromagnetic (EM) enhancement factor,[1, 2] which is usually taken to be proportional to the fourth power of the ratio between the local electric field and the incident field. For systems of spherical particles, the local field can be calculated by the generalized Mie theory,[4, 13] In order to interpret the experimental results above, we simulated the case of a dimer, as shown in Figure 4. The angular variation of the calculated local intensity enhancement is dramatic, as a result of a strongly polarization-dependent coupling between the collective surface plasmon modes of the two Ag particles and the incident field. The variation is strongest for the region between the particles, that is, where the probe molecule should be located due to the self-assembly process leading to dimer formation. At this position, the EM field is enhanced tremendously for polarization parallel to the dimer axis, while the field is instead excluded from the interparticle region for perpendicular polarization. The result is that the local field, the local intensity and the local SERS factor varies as $\cos\alpha$, $\cos^2\alpha$ and $\cos^4\alpha$, respectively, where α is the angle between the dimer axis and the incident electric field vector. However, this angular variation remains even if the various enhancement factors are averaged over the surface of the dimer, as shown in Figure 4 e and 4 f. The reason is that the enhancement in the gap region completely dominates the surface average. These effects, we believe, explain the experimentally observed SERS intensity variation shown in Figure 1 – Figure 3.

More calculations (not shown here) demonstrate that the $\cos\alpha$ polarization dependency in Figure 4 is not sensitive to the particle size, incident wavelength or interparticle separation *d*, as long as the target molecules are located close to the particles; although the absolute magnitude of the enhancement factor depends crucially on these factors.[5] For large interparticle separations, the surface-averaged enhancement factor becomes isotropic, as expected for an isolated sphere. Interestingly, the illumination direction **k** dependency of SERS can be applied to a $\sin^4\alpha$ dependency if the direction of **E** in Figure 4 is instead of the direction of **k**. The reason is that these two cases have the same parallel electric field to the dimer axis: $E_{\|} = E_0 \cdot \cos\alpha$. In the case of nonspherical particles, such as the interacting cylinders investigated by Kottman and Martin[14] or the faceted particles investigated in our previous work,[5] the local field enhancement due to interparticle coupling is qualitatively similar to the case above, and should lead to a similar polarization dependency.

In summary, polarization-dependent Raman-scattering measurements of isolated and identified Ag nanoparticle dimers presented here show that the component of the incident electrical field parallel to the axis of a dimer, that is, $E_{\parallel} = E_0 \cos\alpha$, is the main driving field. The resulting $\cos^4\alpha$ angular dependency is in good agreement with theoretical simulations of the field enhancement around Ag dimers, and the experimental results thus give good support for an interpretation of SERS in terms of an EM enhancement at nanogaps. Recently, Brus and co-workers[16] reached similar conclusions based on investigations of the angular variation of the SERS depolarization ratio for Ag/Rhodamine 6G aggregates. However, the morphologies of the nanoparticle aggregates were not determined, which makes comparisons with theory difficult. One may also note the similarity between the present data and Raman-scattering results for other highly anisotropic and resonant systems, such as oriented carbon nanotubes[17] or CuO chains in high-T_c superconductors.[18] The common denominator in these cases is that an essentially one-dimensional electronic resonance effect singles out one particular polarization component as the driving field for the Raman-scattering process.

Experimental Section and Computational Method

Preparation of colloidal Ag nanoparticles: The Ag hydrosol was prepared by a citrate reduction method, using chemicals of analytic reagent grade. In order to obtain large Ag particles, with an average diameter of around 90 nm, the original protocol of Lee and Meisel[19] was modified as follows: $AgNO_3$ (90 mg) was dissolved in purified (MilliQ) water (650 mL) and 500 mL of this solution was heated to the boiling point, after which a sodium citrate solution (1%, 10 mL) was added. The remaining $AgNO_3$ solution was divided into three parts, which were added 30, 45 and 60 min after the citrate. The solution was then kept boiling for a further 30 min, yielding a final volume of around 500 mL and a nanoparticle concentration of $\approx$35 pM.

Preparation of polymer-coated Si surface, meshed by gold grid: A clean Si wafer was covered by a gold grid with marked 100 μm squares and tightened by pieces of Scotch tape. The wafer was then immersed in a 3-aminopropyltrimethoxysilane (APTMS) methanol solution (10%) for 10 to 12 h, yielding a surface with high affinity to metallic Ag.[20] Using the Au grid, the morphology and orientation of isolated SERS-active Ag aggregates could be determined by SEM.

Hb/Ag mixture: A relatively high concentration (5 nM) of human adult hemoglobin (Sigma) was mixed with the Ag sol in order to achieve efficient aggregation and a high surface coverage. After 3 h of incubation, a droplet of the Hb/Ag solution was deposited on the meshed surface, followed by rinsing in pure water after about one minute. This procedure resulted in the immobilization of well separated Hb/Ag aggregates on the substrate.

Renishaw 2000 micro-Raman setup: Raman spectra were collected in backscattering geometry through a 50× (NA 0.9) objective, using a research grade optical microscope coupled to a single-grating spectrometer equipped with a notch filter and a cooled CCD detector. An argon-ion laser operated at 514.5 nm was used for excitation. A variable incident polarization angle α was obtained by rotating a broad-band half-wave plate mounted on the optical axis common to the collimated incident and scattered beams. The polarization vector of the scattered beam is thus rotated back by the same angle α as the incident beam,[17] which means that the measurements are not affected by the polarization-dependent sensitivity of the spectrometer grating. An analyser and a half-wave plate mounted after the notch filter allowed for selection of polarized or depolarized scattering. Raman images were recorded by focusing the Raman-scattered light directly on the CCD after passing through a 40 nm wide band-pass filter centered at 550 nm. The filter transmits most of the SERS signal but cuts away the main Si phonon at 520 cm^{-1}. A homogenous illumination was obtained by controlling the beam expansion.

Theoretical method: The EM SERS mechanism is based on the enhanced local electric field near the nanoparticle due to the response of the metal surface to the incident field at frequency ω_0 and the Raman-scattered field at frequency $\omega_0 \pm \omega_\nu \approx \omega_0$. The EM SERS enhancement factor can then be approximated by Equation (1):

$$M = M_1(\omega_0) \cdot M_2(\omega_0 \pm \omega_\nu) \approx M_1^2(\omega_0) \quad (1)$$

where $M_1 = [E_{loc}(\omega_0)/E_0(\omega_0)]^2 = I_{loc}(\omega_0)/I_0(\omega_0)$ and E_0, I_0 and I_{loc} are the incident electric field, the incident intensity and the enhanced local intensity, respectively. The local field can be expressed as the sum of the incident field and a scattered field $\mathbf{E_s}$, generated by the response of the electromagnetic environment [Equation (2)]:

$$\mathbf{E_{loc}}(r,\omega) = \mathbf{E_0}(r,\omega) + \mathbf{E_s}(r,\omega) \quad (2)$$

For N coupled spherical particles, the scattered field can be expressed as Equation (3)

$$\mathbf{E_s}(r) = \sum_{i=1}^{N} \mathbf{E_{si}}(r - r_i) = \sum_{i=1}^{N} \sum_{n=1}^{\infty} \sum_{m=-n}^{n} A_{nm}(i) N_{nm}^h(r - r_i) + B_{nm}(i) M_{nm}^h(r - r_i) \quad (3)$$

where $\mathbf{E_{si}}$ is the scattered field from the ith sphere, centered at r_i, and N_{nm}^h and M_{nm}^h are spherical wave vectors in Hankel form. The coefficients A_{nm} and B_{nm}, which depend on the incident polarization and the arrangement of the spheres, can be obtained using the generalized Mie theory, for details see ref. [13].

The authors gratefully acknowledge Juris Prikulis, Dr. K.V.G. K. Murty and Dr. Erik J. Bjerneld for experimental assistance. This work has been supported by the Swedish Foundation for Strategic Research and the Swedish Research Council. One of the authors Xu has been supported by a visiting fellowship from the Nanometer Consortium, Lund University, Sweden.

[1] For a review see, a) M. Moskovits, *Rev. Mod. Phys.* **1985**, *57*, 783; b) A. Otto, in *Light Scattering in Solids IV* (Eds.: M. Cardona, G. Guntherodt), Springer-Verlag, **1984**, 289.
[2] For a review see, a) K. Kneipp, H. Kneipp, I. Itzkan, R. R. Dasari, M. S. Feld, *Chem. Rev.* **1999**, *99*, 2957; b) M. Moskovits, L. L. Tay, J. Yang, T. Haslett, *Top. Appl. Phys.* **2002**, *82*, 215, and references therein.
[3] Y. W. C. Cao, R. C. Jin, C. A. Mirkin, *Science* **2002**, *297*, 1536.
[4] U. Kreibig, M. Vollmer, *Optical Properties of Metal Clusters*, Springer, New York, **1995**.
[5] H. X. Xu, J. Aizpurua, M. Käll, P. Apell, *Phys. Rev. E*, **2000**, *62*, 4318.
[6] H. X. Xu, E. J. Bjerneld, M. Käll, L. Börjesson, *Phys. Rev. Lett.* **1999**, *83*, 4357.
[7] A. M. Michaels, J. Jiang, E. Brus, *J. Phys. Chem. B* **2000**, *104*, 11965.
[8] E. J. Bjerneld, Z. Földes-Papp, M. Käll, R. Rigler, *J. Phys. Chem. B* **2002**, *106*, 1213.

[9] E. J. Bjerneld, H. X. Xu, M. Käll, *Proceedings of the XVIIIth International Conference of Raman Spectroscopy*, Budapest, Hungary, **2002**.
[10] a) P. Etchegoin, H. Liem, R. C. Maher, L. F. Cohen, R. J. C. Brown, M. J. T. Milton, J. C. Gallop, *Chem. Phys. Lett.* **2003**, *367*, 223; b) A. R. Bizzarri, S. Cannistraro, *Appl. Spectrosc.* **2002**, *56*, 1531.
[11] a) A. Otto, *J. Raman Spectrosc.* **2002**, *33*, 593; b) A. Kudelski, B. Pettinger *Chem. Phys. Lett.* **2000**, *321*, 356.
[12] J. de Groot, R. E. Hester, S. Kaminaka, T. Kitagawa, *J. Phys. Chem.* **1988**, *92*, 2044.
[13] H. X. Xu, PhD thesis, Chalmers University of Technology (Sweden), ISBN 91-7291-112-3, **2002**.
[14] a) J. P. Kottmann, O. J. F. Martin, *Opt. Express*, **2001**, *8*, 655; b) J. P. Kottmann, O. J. F. Martin, *Optic. Lett.*, **2001**, *26*, 1096.
[15] P. B. Johnson, R. W. Christy, *Phys. Rev. B*, **1972**, *6*, 4370.
[16] K. A. Bosnick, J. Jiang, L. E. Brus, *J. Phys. Chem. B* **2002**, *106*, 8096.
[17] G. S. Duesberg, I. Loa, M. Burghard, K. Syassen, S. Roth, *Phys. Rev. Lett.* **2000**, *85*, 5436.
[18] M. Käll, M. Osada, M. Kakihana, L. Borjesson, T. Frello, J. Madsen, N. H. Andersen, R. Liang, P. Dosanjh, W. N. Hardy, *Phys. Rev. B*, **1998**, *57*, R14072.
[19] P. C. Lee, D. Meisel, *J. Phys. Chem.* **1982**, *86*, 3391.
[20] R. G. Freeman, K. C. Grabar, K. J. Allison, R. M. Bright, J. A. Davis, A. P. Guthrie, M. B. Hommer, M. A. Jackson, P. C. Smith, D. G. Walter, M. J. Natan, *Science* **1995**, *267*, 1629.

Received: October 17, 2002 [Z544]
Revised: May 13, 2003

Maximum-Likelihood Approach to Single-Molecule Polarization Modulation Analysis

Kenneth D. Osborn,[a] Manoj K. Singh,[a]
Ramona J. Bieber Urbauer,[b] and Carey K. Johnson*[a]

KEYWORDS:

calcium ATPases · calmodulin · fluorescence · molecular dynamics · polarization modulation

Introduction

Single-molecule spectroscopy is increasingly used to probe the dynamics of individual molecules,[1] and spectroscopic techniques that are sensitive to the motion of single molecules are important for detection of these processes. Several single-molecule methods are capable of tracking molecular motions in real time. Fluorescence-intensity trajectories of single molecules can be analyzed to characterize underlying dynamics.[2] Fluorescence resonance energy transfer, which monitors distance changes between two fluorophores,[3–5] can track molecular motions between two dye-labeled sites on a protein. Polarization methods make use of fluorescence polarization to track the orientation of single molecules.[5–9] Polarization methods have been used previously to study reorientational dynamics of fluorescent dyes attached to DNA strands bound to a glass surface.[10–12] These surface studies were sensitive enough to reveal a five-degree offset in the absorption and emission dipoles of the dye Cy5.

Herein, we use a linearly polarized laser of which the orientation of the polarization is continuously varying to excite a dye molecule or an extrinsic fluorophore bound to a protein. The extent to which the fluorescence signal is modulated by the polarization of the excitation beam is a measure of the mobility of the fluorophore on the timescale of the polarization modulation. A fluorophore with fixed orientation experiences maximum excitation when the orientation of the polarization aligns with the transition dipole of the dye and minimum excitation when the polarization is orthogonal to the transition dipole of the dye molecule. Fast reorientation of the transition dipole randomizes the absorption probability, thus eliminating the modulation which is experienced by stationary fluorophores. Tracking the orientational mobility of a fluorophore is thus an effective means of following single-molecule dynamics in real-time.

Single-molecule fluorescence signals are typically recorded as trajectories of fluorescence counts in sequential time bins. Fluorescence counts in these bins are typically at low count levels following Poisson statistics rather than the Gaussian statistics characteristic of higher count levels generated in bulk studies. The signals generated in conventional measurements are often analyzed by least-squares (LS) fitting methods, which are based on Gaussian statistics. These fits can become grossly inaccurate at the signal levels generated by single-molecule experiments for which the data follow a non-Gaussian distribution.[13, 14] In such cases, a maximum-likelihood estimator (MLE) analysis can provide more reliable fits to the data.[15] MLE analysis accounts for the actual number of total counts N, which are distributed following a multinomial distribution among data bins. The likelihood function (L) is given by Equation (1):

$$L = \frac{N!}{n_1!\ldots n_k!} p_1^{n_1} p_2^{n_2} \ldots p_k^{n_k} \quad (1)$$

which describes the probability of N counts being distributed among k channels with n_i counts in channel i (for $i = 1$ to k), where p_i is the normalized probability of finding a count in channel i. The likelihood function attains a maximum for the parametric values corresponding to the best fit of the data. The quotient in the likelihood function accounts for permutations in the random ordering of the counts.

MLE analysis has been widely used to determine fluorescence lifetimes from single-molecule time-correlated single photon counting data,[16, 17] where they provide a means of extracting fluorescence lifetimes from as few as 50 fluorescence counts.[18]

[a] *Prof. C. K. Johnson, K. D. Osborn, M. K. Singh[+]*
Department of Chemistry, University of Kansas
1251 Wescoe Hall Drive, Lawrence, KS 66045 (USA)
Fax: (+1) 785-864-5396
E-mail: ckjohnson@ku.edu.

[b] *R. J. Bieber Urbauer*
Department of Molecular Biology, University of Kansas
1251 Wescoe Hall Drive, Lawrence, KS 66045 (USA)

[+] *Current address:*
Spectroscopy Division
Bhabha Atomic Research Center, Mumbai 400085 (India)

 DOI: 10.1002/cphc.200300677